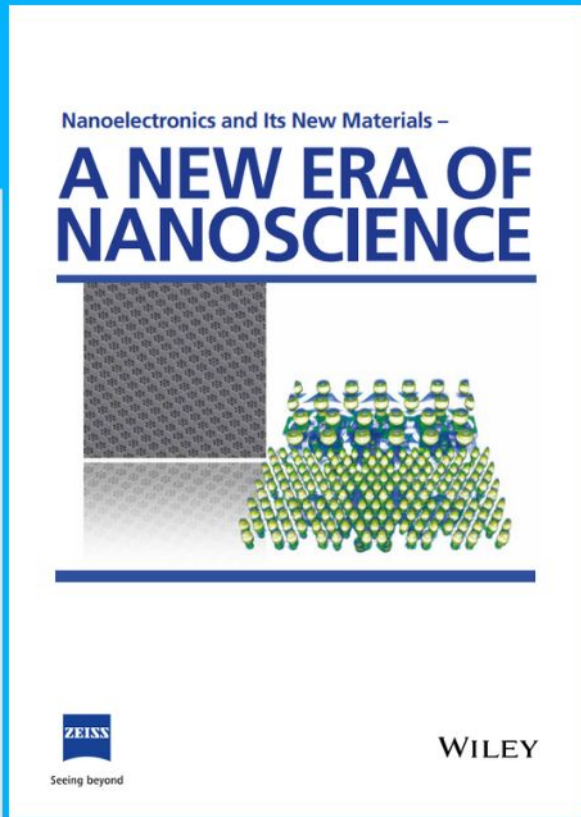




Nanoelectronics and Its New Materials – A NEW ERA OF NANOSCIENCE



Discover the recent advances in electronics research and fundamental nanoscience.

Nanotechnology has become the driving force behind breakthroughs in engineering, materials science, physics, chemistry, and biological sciences. In this compendium, we delve into a wide range of novel applications that highlight recent advances in electronics research and fundamental nanoscience. From surface analysis and defect detection to tailored optical functionality and transparent nanowire electrodes, this eBook covers key topics that will revolutionize the future of electronics.

To get your hands on this valuable resource and unleash the power of nanotechnology, simply download the eBook now. Stay ahead of the curve and embrace the future of electronics with nanoscience as your guide.



Seeing beyond

WILEY

Simple Thermal Annealing-Assisted Direct Synthesis and Optical Property Study of CuO Nanoparticles Incorporated Polyvinyl Alcohol Films

Ram Sevak Singh,* Ram Dayal Patidar, Arun Kumar Singh, Kalim Deshmukh, Kiran Thakur, and Anurag Gautam*

This article reports a simple thermal annealing-assisted direct synthesis method to prepare copper oxide (CuO) nanoparticles incorporated in polyvinyl alcohol (PVA) films and a systematic study of their optical properties. CuO-PVA nanocomposite films are prepared with a different weight percentage of CuO in the PVA matrix. Scanning electron microscopy (SEM), X-ray diffraction (XRD), UV-visible spectroscopy, and photoluminescence spectroscopy are employed to study the prepared films. XRD confirms the formation of crystalline CuO nanoparticles in PVA, while the SEM analysis shows uniformly distributed spherical nanoparticles in PVA. The findings show that thermal annealing at a mild temperature plays a crucial role in improving the crystallinity and optical properties of the nanocomposite film. In comparison to PVA, CuO-PVA nanocomposite exhibits improved absorption with a new absorption band in the lower wavelength region. The nanocomposite samples excited with 300 nm show intense photoluminescence (PL) at 365 nm and an increase of PL intensity with CuO concentration in the PVA matrix. In contrast, samples excited with 425 nm show green emission at 550 nm in the visible region of the electromagnetic spectrum. The PL in CuO-PVA nanocomposites can be originated due to the transitions associated with acceptor and donor defects in the material. The study opens up a new route to fabricate CuO-PVA nanocomposites with superior optical properties.

supercapacitors, batteries, and optical sensors.^[2] Metal oxides in bulk forms lack many physical and chemical properties, compared to their nanostructures which offer many advantages including high surface area and chemical reactivity, novel optical and electrical properties.^[3–6] Various metal oxides such as ZnO, NiO, CuO, Co₃O₄, Fe₃O₄, CeO₂, TiO₂, etc. in their nanoforms have been synthesized and applied in various applications such as catalysis, sensors, biosensors, and biomedical engineering fields.^[1,7,8] Among them, copper oxide (CuO) nanoparticles are more attractive due to their nontoxicity and fascinating tunable electrical and optical properties.^[4] They also possess excellent antiviral and antibacterial properties.^[9] Interestingly, CuO nanoparticles can kill the COVID-19 virus^[10] and can be embedded into a respiratory mask to improve its function against antiviral infection.^[11]


CuO is a semiconductor and has a monoclinic crystal structure.^[11,12] In this phase, it has outstanding photochemical and photoconductive properties, which have promising applications in solar cells and photodetectors.^[4,13–16] The physical and chemical behaviors of CuO are sensitive to the structure of the nanomaterial and the composition of the material. As such, photoluminescence and other properties of CuO can be tuned by reducing its size to nanoscales.^[12,13] Further, photoluminescence and optical absorption properties change with the size, shape, and stoichiometry of

1. Introduction

Metallic nanoparticles, their oxides, and composites have been largely investigated and utilized in the area of science and engineering.^[1] They possess excellent physiochemical properties desired for applications in solar cells, photodetectors,

R. S. Singh, K. Thakur
Department of Physics
OP Jindal University
Raigarh, Chhattisgarh 496109, India
E-mail: singh915@gmail.com

R. D. Patidar
Department of Electrical Engineering
OP Jindal University
Raigarh, Chhattisgarh 496109, India

 The ORCID identification number(s) for the author(s) of this article can be found under <https://doi.org/10.1002/pssa.202300328>.

DOI: 10.1002/pssa.202300328

A. K. Singh
Department of Pure and Applied Physics
Guru Ghasidas Vishwavidyalaya
Bilaspur, Chhattisgarh 495009, India

K. Deshmukh
New Technologies-Research Center
University of West Bohemia
30100 Plzeň, Czech Republic

A. Gautam
School of Sciences
Malla Reddy University
Dulapally, Hyderabad 500100, Telangana, India
E-mail: ganurag13@gmail.com

nanoparticles and the methods of their synthesis.^[13,17–19] Polyvinyl alcohol (PVA) is a low-cost and semicrystalline biocompatible polymer that is transparent and has good mechanical strength.^[20–23] Physicochemical properties of PVA can further be altered by incorporating CuO into PVA, which may result in new or improved optical, electrical, and mechanical properties depending on the method of preparation and concentration of CuO in PVA.^[13,24–27] Reported methods to synthesize CuO nanoparticles include microwave irradiation,^[28] chemical coprecipitation,^[29] sol–gel^[30] sonochemical,^[31] and combustion.^[32] These methods undergo complicated processes and use expensive materials and equipment. Rao et al.^[25] reported the dielectric properties of CuO-PVA nanocomposite films. They used many complicated multiple steps to prepare the nanocomposites. First, a powder of CuO nanoparticles was prepared using the combustion method followed by calcinations at relatively high temperature of 400 °C. Then, nanocomposite films were prepared by an additional casting method. Alhazime et al.^[33] reported the thermal and optical absorption properties of CuO nanoparticles doped PVA-polyethylene glycol (PEG) polymer. They first prepared CuO nanoparticles using multiple steps in the sol–gel method and thereafter CuO-PVA-PEG blends were prepared. Complicated multiple steps were adopted in this study and photoluminescence (PL) properties were also not explored. Recently, Noor Al-Huda Al-Aaraji et al.^[13] reported enhanced optical absorption ($\approx 62.2\%$) in silicon carbide/CuO/PVA nanocomposite with a substantial reduction of the bandgap in PVA. However, the PL study was not conducted in this report. More recently, the electrical properties and optical absorption of CuO/PVA nanocomposites synthesized using the green method were reported.^[4] They observed not only the narrowing of energy gap but also the improvement in the DC conductivity in PVA after CuO nanoparticles are doped into PVA. This report also lacks the PL investigations of the nanocomposites. Recently, Kaur et al.^[34] reported the CuO/PVA flexible composite materials for microwave reflection application. In another report,^[35] CuO/PVA nanocomposites showed high photocatalytic activity for the degradation of rhodamine B dye. In this direction, the development of a simple, eco-friendly, and inexpensive method to prepare CuO-PVA nanocomposites and the study of their not only optical absorption but also photoluminescence properties are still needed to improve and produce novel optical properties.

Here, we report a simple route to prepare inexpensive CuO-PVA nanocomposite films and study their optical absorption and photoluminescence properties. The method of synthesis and optical properties observed in this study are significantly different and have many advantages over previous reports. Synthesis of the nanocomposite films undergoes just one step followed by thermal annealing at a mild temperature to improve their structural and optical properties. The method is compatible with the mass production of CuO-PVA nanocomposite films. Intense photoluminescence observed in both ultraviolet and visible green light widens the applications of the nanocomposite films in optoelectronics, photoluminescence-based sensors, and imaging systems, and the fabrication of low-cost ultraviolet and visible light sources.

2. Experimental Section

2.1. Synthesis

Cuprous chloride (CuCl) and polyvinyl alcohol (PVA) were purchased from Loba Chemie Pvt. Ltd., and were used as a precursor for CuO nanoparticles and polymer matrix respectively in the synthesis of CuO-PVA nanocomposite films. In a typical synthesis process, the first PVA solution was prepared by dissolving 2 g of PVA in distilled water in a round bottom flask. Subsequently, the flask containing the PVA solution with a magnetic bar was placed in the water bath that was sitting on a hot plate with a magnetic stirrer. The water bath heating was conducted at a temperature of $\approx 55\text{--}60$ °C until the PVA solution becomes transparent. Thereafter, a calculated wt% of CuCl was mixed in the hot solution under stirring and the steering of the hot mixture was continued for 8 h. The color of the mixture solution changes during the synthesis process, as shown in the upper panel of **Figure 1**. Initially, the color of CuCl-contained PVA solution was light green which changes from brownish to milky green as the final color. The excess water in the solution was further evaporated to make the solution more viscous. To prepare thin films the viscous solution was poured into a Petri dish and held to dry overnight and finally, the film was detached from the pot for further processing. Using this method, the films with four different concentrations of CuCl were prepared. Further, all the as-prepared films were thermally annealed at a mild temperature of 140 °C for 45 min to obtain CuO-PVA nanocomposite films. After annealing, the color of the CuO-PVA film became slightly brownish while bare PVA remained transparent, as shown in **Figure 1**.

2.2. Characterization

To confirm the formation, and study of the phase and crystal structure of CuO-PVA nanocomposite films, an X-ray diffractometer (Regaku, wavelength of X-rays = 1.54 Å). The scan rate used to accomplish the X-ray diffraction analysis was $0.02^\circ \text{ min}^{-1}$. Additionally, the shapes and sizes of nanoparticles were characterized using a field-emission scanning electron microscope (model: FEI-Apreo S). UV-visible spectroscopy measurements were conducted with a Shimadzu UV-visible spectrometer in the 200–800 nm wavelength range to study the optical absorption property and calculation of optical bandgap E_g . Photoluminescence spectra were acquired from CuO-PVA nanocomposite films using high sensitivity fluorescence spectrometer (Model: FL-100-HS, MARUTEK) with excitation wavelengths of 300 and 425 nm.

3. Results and Discussion

3.1. XRD Analysis

Figure 2 shows the XRD patterns of CuO-PVA films with four different wt% of CuO in the PVA matrix. PVA film exhibits a broad peak at $2\theta = 18.9^\circ$ that is indexed to the (101) crystal plane of PVA, which is in agreement with our previous findings.^[36]

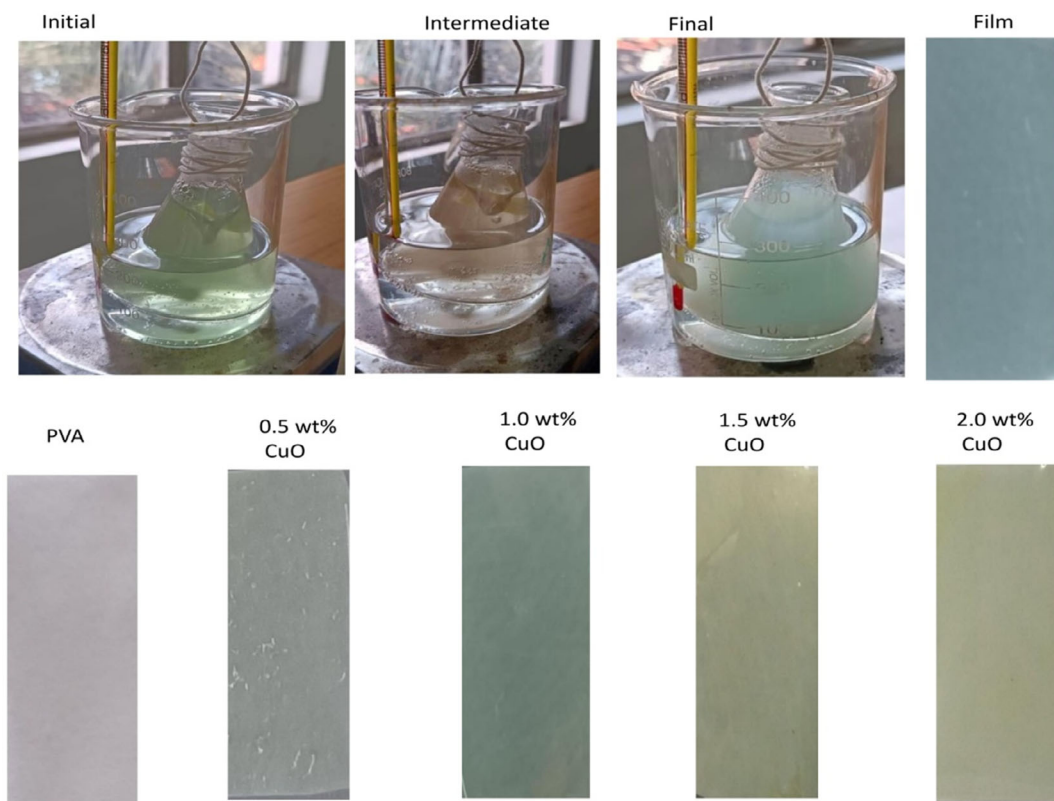


Figure 1. Upper panel: Color changes of solution (initial, intermediate, and final) during the synthesis process of CuO nanoparticles incorporated PVA and subsequently prepared film. Lower panel: PVA film and different PVA-CuO nanocomposite films annealed at 140 °C.

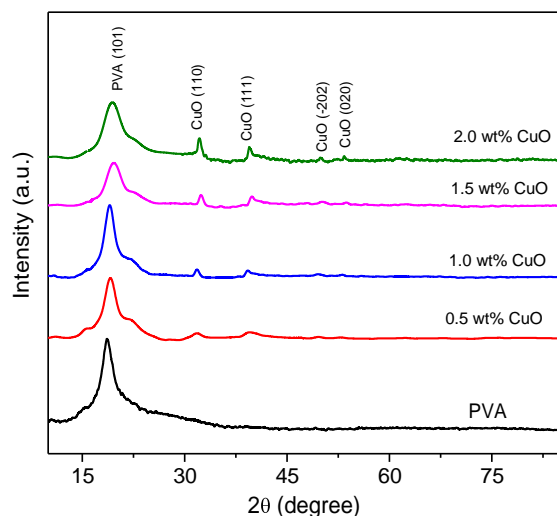


Figure 2. XRD patterns of CuO-PVA nanocomposite films with varying wt% of CuO in PVA film.

A relatively broad peak of PVA indicates that it is semicrystalline. Crystallinity in PVA is caused by intermolecular polymer chain interactions between the PVA and cross-linking between the different polymorphs of the PVA such as syndiotactic, isotactic, and atactic forms. XRD patterns of CuO-PVA films show the

appearance of new sharp peaks (full width at half maximum $<0.5^\circ$) at $2\theta = 32.36^\circ$, 39° , 49° , and 53.50° which correspond to the (110), (111), (-202) , and (020) crystal planes of monoclinic CuO and validate the formation of the nanoparticles incorporated in the PVA films^[35] (JCPDS card number 45-0937). It is also noteworthy that the intensity of CuO peaks increases with the increase of CuO content in PVA film. Additionally, XRD pattern does not have any impurity peak in the diffractogram. The lattice parameters calculated from XRD data are $a = 4.6770 \text{ \AA}$, $b = 3.4221 \text{ \AA}$, and $c = 5.1422 \text{ \AA}$, which are well agreeing with the values reported in the literature.^[33] The calculated average crystallite size for 2 wt% CuO in PVA is $\approx 16 \text{ nm}$ calculated using the Scherrer formula given below

$$L = 0.9\lambda/\beta \cos \theta \quad (1)$$

where L is crystallite size, β and λ are full width at half maxima (FWHM) and the wavelength of X-rays, respectively.

To assess the influence of annealing at 140 °C, we also conducted the XRD measurement of a 2 wt% CuO-PVA film before annealing and compared it with the sample after annealing, as shown in **Figure 3**. It is seen that the film, before annealing, exhibits weak CuO peaks in XRD pattern. In contrast, the CuO peak is pronounced after annealing, indicating thermal-assisted nucleation and further reduction to form more crystalline CuO nanoparticles in PVA film. These results are in good agreement with the change in the crystallinity of Ag-PVA

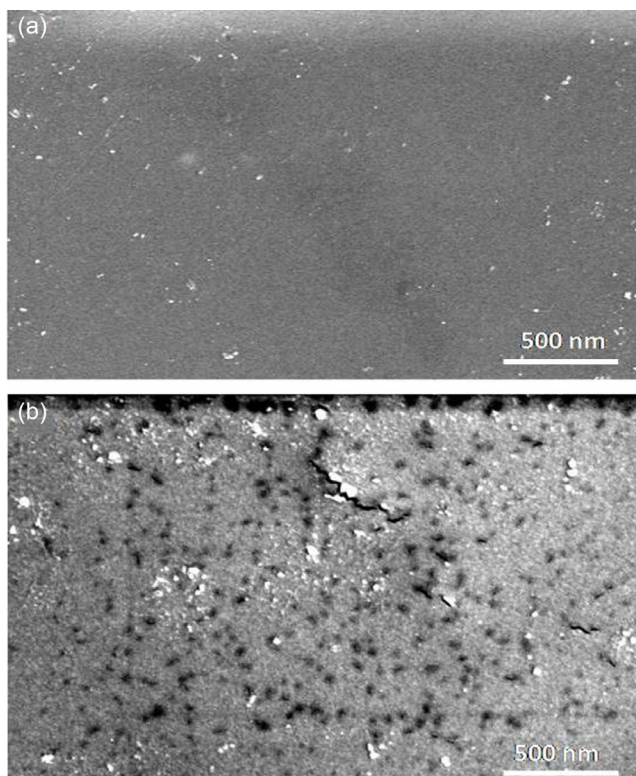


Figure 3. SEM pictures of a) bare PVA film and b) 2 wt% CuO-PVA film.

nanocomposite films before and after heat treatment.^[36] It is noticed that crystallite size is also improved from 12 to 16 nm after the thermal annealing, which agreed with the previously published reports^[37,38] where thermal annealing improved the crystallite size of CuO nanoparticles. This implies that thermal annealing is playing a crucial role in the synthesis of CuO-PVA nanocomposite films.

3.2. SEM Analysis

Figure 3 shows the SEM images of the bare PVA film (Figure 3a) and a 2 wt% CuO-PVA film (Figure 3b). The SEM image of bare PVA film shows a clean surface and does not have any particle-like structure visible in the image. However, blackish particles of sizes in the range of ≈ 50 – 100 nm uniformly distributed in the film are visible in Figure 3b, confirming the formation of CuO nanoparticles in PVA film. We also notice that the shapes of particles are slightly distorted from spherical-shaped particles visible in the sample before annealing (see Figure 4), which can be attributed to the thermal expansion or contraction of particles after annealing. The surface also looks different after annealing, showing the change in surface morphology as well after the thermal annealing.

These changes in the shape, size, or morphology of nanoparticles may also contribute to the alteration of optical properties of the nanocomposite films.

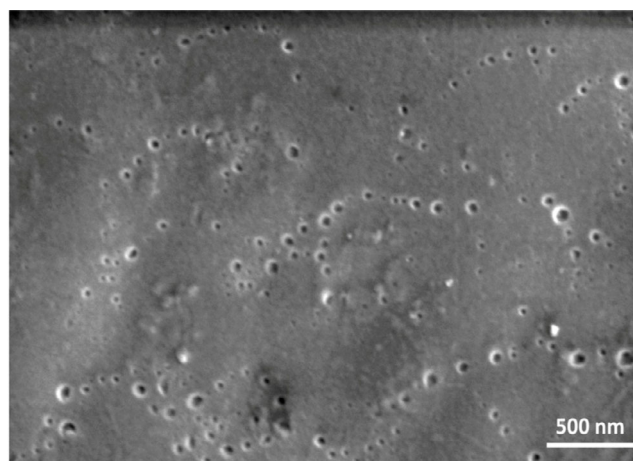


Figure 4. SEM of 2 wt% CuO-PVA film before annealing.

3.3. UV-Visible Analysis

Figure 5 shows the UV-visible absorption spectra of the bare PVA film and CuO-PVA composite films consisting of different wt% of CuO. The PVA has a strong absorption at ≈ 245 nm. CuO-PVA nanocomposite films show the appearance of a new absorption band at ≈ 263 nm, which indicates the incorporation of CuO nanoparticles in the PVA matrix. This absorption band may account for the impurity levels introduced in PVA due to CuO doping. Further, we also notice that CuO doping in PVA modulates the optical properties significantly, showing the increase of absorbance with an increase of CuO concentration in PVA and changes in absorption edges. Changes in absorption edges indicate a reduction in the bandgap.

To get more insight into the observed optical properties, we calculated the optical energy gap E_g of PVA and CuO-PVA films using the following Tauc equation^[4,39]

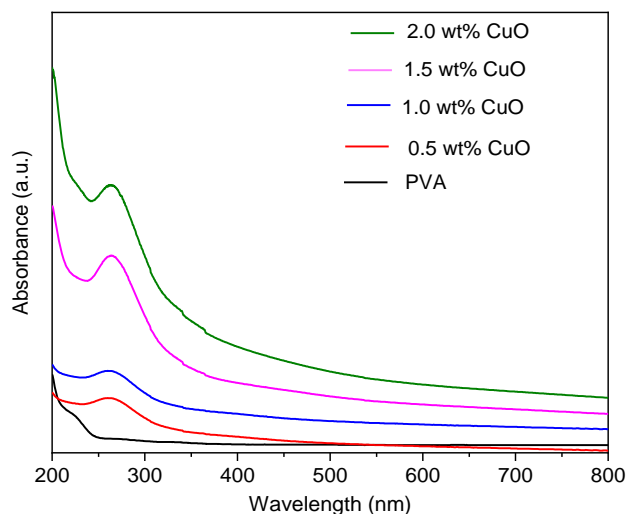


Figure 5. UV-visible absorption spectra of bare PVA film and CuO-PVA nanocomposite films with varying wt% of CuO in PVA.

$$(\alpha E)^n = B(E - E_g) \quad (2)$$

where E is photon energy, α is absorption coefficient (which is A/x , A is absorbance measured in Figure 5, x is film thickness), B is a constant, and E is the energy of the photon. n is 2 for the direct bandgap and $1/2$ for the indirect bandgap. Thus, Tauc plots for direct bandgap can be produced, and the extrapolations of the graph's interesting x -axis, where y -axis value = 0 will be estimated as E_g . The Tauc plots generated from Figure 5 are presented in Figure 6. From Figure 6, the bandgap of the bare PVA is estimated to be ≈ 5.1 eV. Similarly, the bandgaps of the nanocomposite films containing different wt% of CuO in PVA can be estimated, which are 4.0, 3.87, 3.81, and 3.75 eV for the films containing 0.5 wt% CuO, 1.0 wt% CuO, 1.5 wt% CuO, and 2.0 wt% CuO in PVA, respectively. It is noticed that the bandgap of nanocomposite film is reduced with an increase of CuO nanoparticles content in the composite. The optical bandgap reduction can be understood as follows. When nanoparticles of CuO are introduced into the PVA, it generates impurity levels in the energy gap, which account for redshifts in the absorption spectrum corresponding to the narrowing in the bandgap.

Figure 7 shows the influence of annealing on the UV-visible spectrum of 2.0 wt% CuO-PVA films. The annealed film shows the enhanced absorbance and reduction of E_g (from 3.85 to 3.75 eV) which could be caused by an increase in crystalline CuO nanoparticles under the influence of annealing, which is supported by the XRD patterns (Figure 8).

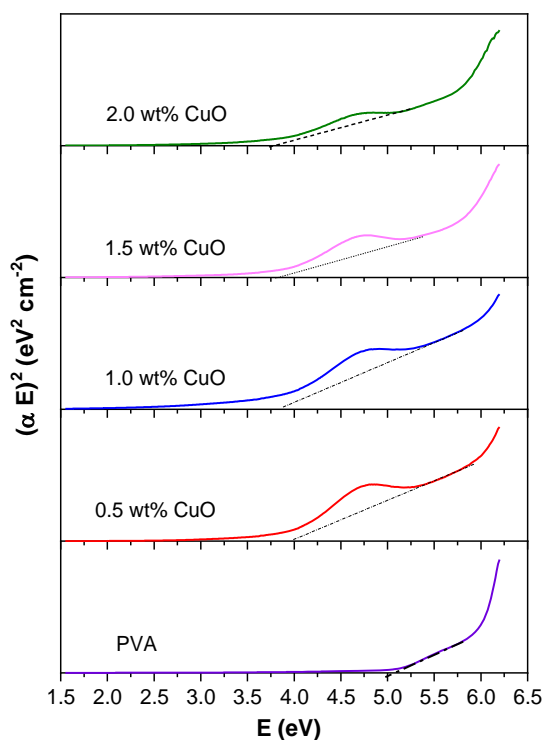


Figure 6. Tauc plots generated from Figure 6 show the values of E_g of bare PVA and CuO-PVA nanocomposite films with varying wt% of CuO in PVA.

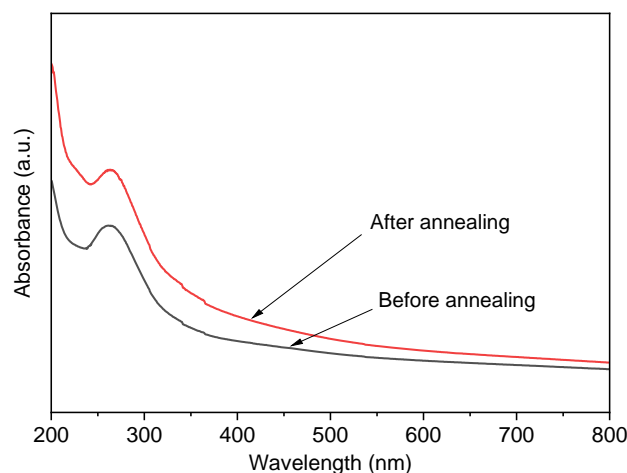


Figure 7. UV-visible spectra of 2 wt% PVA-CuO nanocomposite film before annealing and after annealing at 140 °C.

3.4. Photoluminescence (PL) Analysis

PL spectra acquired from the bare PVA film and CuO-PVA nanocomposite films with different wt% of CuO at the 300 nm excitation wavelength (λ_{ex}) are shown in Figure 9. Concerning the bare PVA, CuO-PVA nanocomposite films show intense PL peak at 365 nm in the UV region, and PL intensity increases with the increase of wt% of CuO nanoparticles in PVA. It is realized that emission is mainly due to the CuO nanoparticles. The emission in the UV region indicates near band-edge emission caused by excitonic electron-hole recombination in CuO. Further, CuO-PVA films excited at 425 nm show an emission peak centered at ≈ 550 nm which is a green emission (Figure 10). It is in good agreement with the previous findings of CuO nanoparticles prepared with the help of copper acetate and sodium hydroxide at 100 °C.^[40] The peak in the green emission arises from the singly ionized oxygen vacancy. Further, the intensity of the PL increases in proportion to the increase in CuO nanoparticles content in PVA. However, no PL was observed at 425 nm excitation wavelength in bare PVA, which is supported with the literature.^[41]

It has been found that the bulk CuO is not luminescent. However, CuO in its nanoscale form emits light in visible and UV regions.^[40,42,43] which is well agreed with the observed PL in our study. PL emission in CuO can be originated due to the presence of acceptor and donor defects in CuO. These defects could be oxygen or copper vacancies and interstitial copper or oxygen sites.^[41,44–46] The presence of defects in CuO introduces new energy levels within the energy gap, as shown in Figure 11.

The mechanism of PL in CuO-PVA can be understood as follows. When light is incident on the sample, electrons are excited to a higher energy conduction band (CB) as presented by black arrows in Figure 11. These excited electrons can undergo relaxation through nonradiative transitions from CB to the donor defect levels (red arrows in Figure 11) and then they recombine with holes by radiative transitions from donor defect levels to either the acceptor defect levels or valence band (VB) sublevels

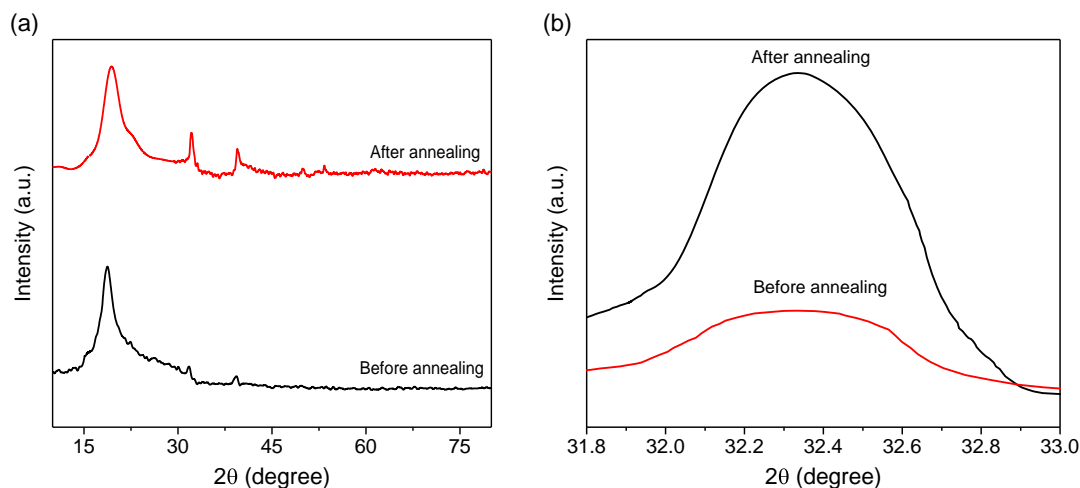


Figure 8. a) XRD patterns of 2 wt% PVA-CuO nanocomposite film before annealing and after annealing at 140 °C. b) High-resolution XRD peak of CuO at lower angle acquired from 2 wt% PVA-CuO nanocomposite film.

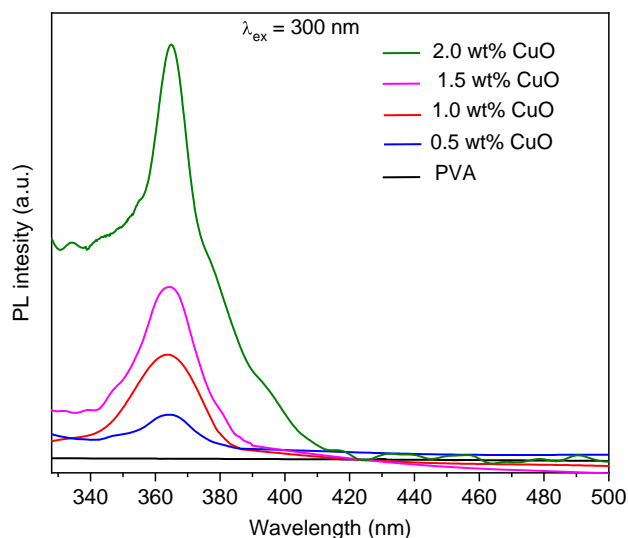


Figure 9. PL spectra (excitation wavelength $\lambda_{\text{ex}} = 300 \text{ nm}$) acquired from the bare PVA and PVA-CuO nanocomposite films of varying content of CuO in PVA film, showing the emission peak centered at 365 nm.

(see green arrows in Figure 11), which results in emission spectra in visible and UV regions.

The influence of thermal annealing on the PL property of a CuO-PVA film is presented in **Figure 12**. It is clear that the as-prepared CuO-PVA film shows very weak PL while the annealing of CuO-PVA films enhances the PL in both UV and visible regions because the thermal annealing stimulates reduction and hence nucleation, formation, and crystallization of more CuO nanoparticles. An increase in crystallinity may improve PL as a more ordered state avoids quenching induced by atomic or molecular collisions. Thus, this method of synthesis using thermal annealing is new and it improves not only the structural property but also the optical absorbance, bandgap, and photoluminescence of the nanocomposite films.

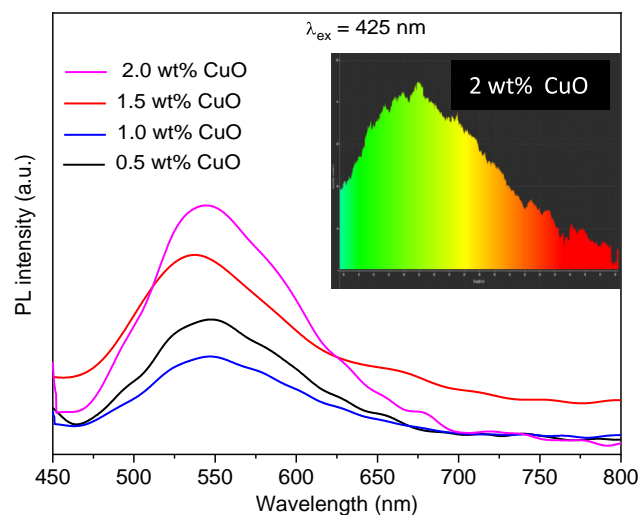


Figure 10. PL spectra ($\lambda_{\text{ex}} = 425 \text{ nm}$) acquired from PVA-CuO nanocomposite films of varying wt% of CuO in PVA film, showing the emission peak centered at 550 nm (green light). The inset shows the color spectrum of the 2 wt% CuO-PVA nanocomposite film.

Down conversion (DC) is another important process in solar cells such as organic solar cells (OSCs) and dye-sensitized solar cells (DSSC) to improve their efficiency.^[47,48] In DC, high-energy photons are converted into low-energy photons, similar to our case where high-energy photons with wavelengths of 300 and 425 nm are converted into lower-energy photons of wavelengths 365 and 550 nm, respectively. This suggests that CuO-PVA nanocomposites may also be utilized as DC materials in DSSC.

4. Conclusion

In summary, CuO-PVA nanocomposite films with different wt% of CuO in PVA were synthesized using a simple one-step process

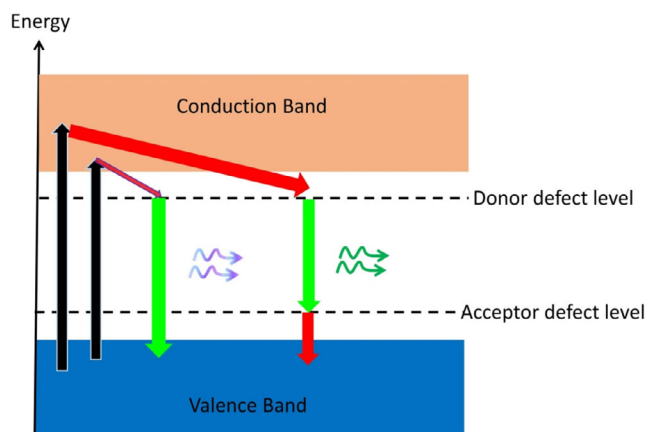


Figure 11. Proposed mechanism of PL. Red arrows represent nonradiative transitions and green arrows represent radiative transitions. The black arrows show excitations of electrons from the valence band to the conduction band.

followed by thermal annealing at a mild temperature of 140 °C. The synthesized films were studied using an X-ray diffraction technique, scanning electron microscope, UV-visible spectroscopy, and photoluminescence spectroscopy. The findings show that thermal annealing assists in the nucleation and growth of crystalline CuO nanoparticles and improves the optical properties of the nanocomposite film. Compared with the bare PVA, the CuO-PVA nanocomposite films show enhanced optical absorption and reduction of energy gap from 5.2 eV of the pristine PVA to 3.75 eV of PVA doped with 0.2 wt% CuO. The composite film excited at 300 nm exhibits a photoluminescence (PL) peak at 365 nm in the UV region and the intensity of the PL increases with an increase in wt% of CuO nanoparticles in PVA. In contrast, CuO-PVA nanocomposite excited at 425 nm shows strong green emission at 550 nm, and emission intensity is further pronounced when the concentration of CuO is increased in PVA. UV and visible PL are produced due to the transitions associated with acceptor and donor defects present in CuO nanoparticles. The thermal annealing-assisted direct synthesis of

CuO-PVA nanocomposite films and its optical properties have the potential for the mass fabrication of low-cost nanocomposite films in a wide range of applications including solar cells, photodetectors, and photocatalysts, down conversion in organic and dye-sensitized solar cells, photoluminescence-based optical sensors, biosensors, antiviral and antibacterial activities, supercapacitors and batteries.

Acknowledgements

The authors acknowledge OP Jindal University, Raigarh, India to provide research facilities including X-ray diffractometer, fluorescence spectrometer, and other support to conduct this research.

Conflict of Interest

The authors declare no conflict of interest.

Data Availability Statement

Data sharing is not applicable to this article as no new data were created or analyzed in this study.

Keywords

absorption spectra, CuO-PVA nanocomposite films, green emission, thermal annealing, ultraviolet emission

Received: April 27, 2023
Revised: June 20, 2023
Published online: August 2, 2023

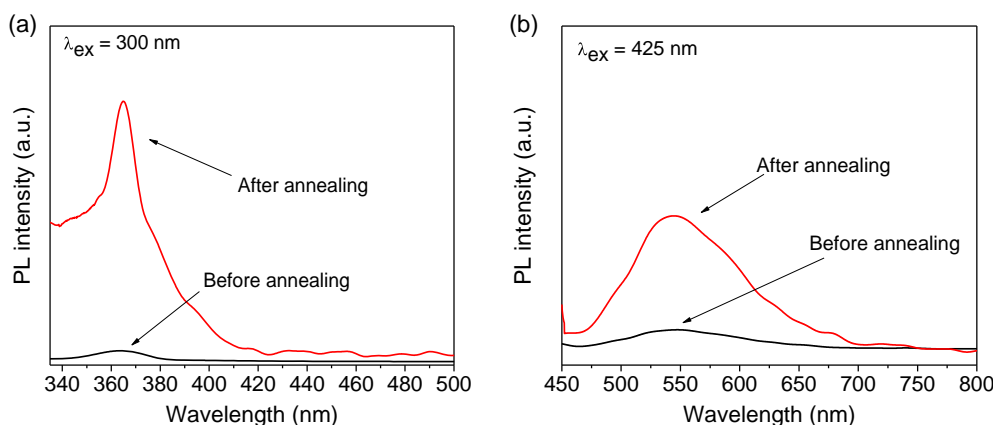


Figure 12. PL spectra of 2 wt% PVA-CuO nanocomposite film before annealing and after annealing at 140 °C at excitation wavelengths (λ_{ex}) of a) 300 nm and b) 425 nm.

- [5] R. S. Singh, A. Rasheed, A. Gautam, A. K. Singh, V. Rai, *Russian J. Appl. Chem.* **2021**, *94*, 402.
- [6] R. S. Singh, D. Li, Q. Xiong, I. Santoso, X. Yu, W. Chen, A. Rusydi, A. T. S. Wee, *Carbon* **2016**, *106*, 330.
- [7] R. Medhi, M. D. Marquez, T. R. Lee, *ACS Appl. Nano Mater.* **2020**, *3*, 6156.
- [8] R. S. Singh, A. Gautam, V. Rai, *Iran. J. Chem. Chem. Eng.* **2023**, *42*, 731.
- [9] A. Waris, M. Din, A. Ali, M. Ali, S. Afridi, A. Baset, A. U. Khan, *Inorg. Chem. Commun.* **2021**, *123*, 108369.
- [10] Z. Fakhroueian, P. Esmailzadeh, P. Esmailzadeh, Preprints.org **2020**, 2020070443.
- [11] J. Zhou, Z. Hu, F. Zabihi, Z. Chen, M. Zhu, *Adv. Fiber Mater.* **2020**, *2*, 123.
- [12] S. Dagher, Y. Haik, A. I. Ayesh, N. Tit, *J. Lumin.* **2014**, *151*, 149.
- [13] N. A.-H. Al-Aaraji, A. Hashim, A. Hadi, H. M. Abduljalil, *Silicon* **2022**, *14*, 10037.
- [14] M. Rokhmat, E. Wibowo, M. Abdullah, *Procedia Eng.* **2017**, *170*, 72.
- [15] T. Gnanasekar, S. Valanarasu, I. L. P. Raj, P. Mohanraj, M. Ubaidullah, S. F. Shaikh, M. S. Tamboli, *Opt. Mater.* **2022**, *124*, 112006.
- [16] W. Tian, C. Zhi, T. Zhai, X. Wang, M. Liao, S. Li, S. Chen, D. Golberg, Y. Bando, *Nanoscale* **2012**, *4*, 6318.
- [17] K. K. Dey, P. Kumar, R. R. Yadav, A. Dhar, A. K. Srivastava, *RSC Adv.* **2014**, *4*, 10123.
- [18] S. Rehman, A. Mumtaz, S. Hasanain, *J. Nanopart. Res.* **2011**, *13*, 2497.
- [19] A. El-Trass, H. ElShamy, I. El-Mehasseb, M. El-Kemary, *Appl. Surf. Sci.* **2012**, *258*, 2997.
- [20] S. Sau, S. Pandit, S. Kundu, *Surf. Interfaces* **2021**, *25*, 101198.
- [21] A. Gautam, P. Komal, R. S. Singh, P. Gautam, S. Manjari, R. Ningthoujam, *J. Mol. Liq.* **2021**, *334*, 116112.
- [22] A. Gautam, P. Komal, *J. Nanosci. Nanotechnol.* **2019**, *19*, 8071.
- [23] A. Gautam, A. Sharma, R. S. Singh, P. Gautam, *Iran. J. Chem. Chem. Eng.* **2022**, <https://doi.org/10.30492/IJCC.E.2022.551274.5266>.
- [24] J. Pulit-Prociak, A. Staroń, P. Staroń, A. Chmielowiec-Korzeniowska, A. Drabik, L. Tymczyna, M. Banach, *J. Nanobiotechnol.* **2020**, *18*, article no. 148.
- [25] J. K. Rao, A. Raizada, D. Ganguly, M. M. Mankad, S. Satyanarayana, G. Madhu, *J. Mater. Sci.* **2015**, *50*, 7064.
- [26] J. K. Rao, A. Raizada, D. Ganguly, M. M. Mankad, S. Satyanarayana, G. Madhu, *Polym. Bull.* **2015**, *72*, 2033.
- [27] Z. Malik, A. Khattak, A. A. Alahmadi, S. U. Butt, *Mater.* **2022**, *15*, 5154.
- [28] H. Wang, J.-Z. Xu, J.-J. Zhu, H.-Y. Chen, *J. Cryst. Growth* **2002**, *244*, 88.
- [29] T. Jan, S. Azmat, Q. Mansoor, H. Waqas, M. Adil, S. Ilyas, I. Ahmad, M. Ismail, *Microb. Pathog.* **2019**, *134*, 103579.
- [30] F. Wang, H. Li, Z. Yuan, Y. Sun, F. Chang, H. Deng, L. Xie, H. Li, *RSC Adv.* **2016**, *6*, 79343.
- [31] N. Wongpisutpaisan, P. Charoonsuk, N. Vittayakorn, W. Pecharapa, *Energy Procedia* **2011**, *9*, 404.
- [32] N. Pavithra, K. Manukumar, R. Viswanatha, G. Nagaraju, *Inorg. Chem. Commun.* **2021**, *130*, 108689.
- [33] A. A. Alhazime, *J. Inorg. Organomet. Polym. Mater.* **2020**, *30*, 4459.
- [34] H. Kaur, R. Prasad, K. Parashar, S. Parashar, presented at *AIP Conf. Proc.*, Vol. 2740, American Institute of Physics, USA **2023**, p. 060003.
- [35] Z. A. Mahar, G. Q. Shar, A. Balouch, A. H. Pato, A. R. Shaikh, *New J. Chem.* **2021**, *45*, 16500.
- [36] A. Gautam, P. Tripathy, S. Ram, *J. Mater. Sci.* **2006**, *41*, 3007.
- [37] S. Panigrahi, S. Kundu, S. Ghosh, S. Nath, T. Pal, *J. Nanopart. Res.* **2004**, *6*, 411.
- [38] A. Gautam, S. Ram, *J. Alloys Compd.* **2008**, *463*, 428.
- [39] C. Vidyasagar, Y. Arthoba Naik, T. Venkatesha, R. Viswanatha, *Nano-Micro Lett.* **2012**, *4*, 73.
- [40] A. S. Lanje, S. J. Sharma, R. B. Pode, R. S. Ningthoujam, *Adv. Appl. Sci. Res.* **2010**, *1*, 36.
- [41] J. Mieloszyk, R. Drabent, J. Siódmiak, *J. Appl. Polym. Sci.* **1987**, *34*, 1577.
- [42] C. Vidyasagar, Y. A. Naik, T. Venkatesh, R. Viswanatha, *Powder Technol.* **2011**, *214*, 337.
- [43] R. S. Singh, R. Y. Tay, W. L. Chow, S. H. Tsang, G. M. Mallick, E. H. T. Teo, *Appl. Phys. Lett.* **2014**, *104*, 163101.
- [44] D. I. Son, C. H. You, T. W. Kim, *Appl. Surf. Sci.* **2009**, *255*, 8794.
- [45] J. Koshy, M. S. Samuel, A. Chandran, K. George, presented at *AIP Conf. Proc.*, Vol. 1391, American Institute of Physics, USA **2011**, p. 576.
- [46] N. Horti, M. Kamatagi, S. Nataraj, presented at *AIP Conf. Proc.*, Vol. 2740, American Institute of Physics, USA **2019**, p. 060003.
- [47] R. Datt, S. Bishnoi, H. K. H. Lee, S. Arya, S. Gupta, V. Gupta, W. C. Tsoi, *Aggregate* **2022**, *3*, 185.
- [48] J. Liu, Q. Yao, Y. Li, *Appl. Phys. Lett.* **2006**, *88*, 173119.